
Article:
Panyasantisuk, J., Dall'Ara, E. orcid.org/0000-0003-1471-5077, Pretterklieber, M. et al. (2 more authors) (2018) Mapping anisotropy improves QCT-based finite element estimation of hip strength in pooled stance and side-fall load configurations. Medical Engineering and Physics, 59. pp. 36-42. ISSN 1350-4533

https://doi.org/10.1016/j.medengphy.2018.06.004

Mapping anisotropy improves QCT-based finite element estimation of hip strength in pooled stance and side-fall load configurations

J. Panyasantisuk[a], E. Dall'Ara[b], M. Pretterklieber[c], D. H. Pahr[d], P. K. Zysset[a,*]

[a]*Institute for Surgical Technology and Biomechanics, University of Bern, Switzerland*
[b]*Department of Oncology and Metabolism and INSIGNEO, Institute for in silico Medicine, University of Sheffield, United Kingdom*
[c]*Division of Anatomy, Medical University of Vienna, Austria*
[d]*Institute for Lightweight Design and Structural Biomechanics, Vienna University of Technology and Department for Anatomy and Biomechanics, Karl Landsteiner Private University for Health Sciences, Austria*

Abstract

Hip fractures are one of the most severe consequences of osteoporosis. Compared to the clinical standard of DXA-based aBMD at the femoral neck, QCT-based FEA delivers a better surrogate of femoral strength and gains acceptance for the calculation of hip fracture risk when a CT reconstruction is available. Isotropic, homogenised voxel-based, finite element (hvFE) models are widely used to estimate femoral strength in cross-sectional and longitudinal clinical studies. However, fabric anisotropy is a classical feature of the architecture of the proximal femur and the second determinant of the homogenised mechanical properties of trabecular bone. Due to the limited resolution, fabric anisotropy cannot be derived from clinical CT reconstruc-

*Corresponding author
Email address: philippe.zysset@istb.unibe.ch (P. K. Zysset)

tions. Alternatively, fabric anisotropy can be extracted from HR-pQCT images of cadaveric femora. In this study, fabric anisotropy from HR-pQCT images was mapped onto QCT-based hvFE models of 71 human proximal femora for which both HR-pQCT and QCT images were available. Stiffness and ultimate load computed from anisotropic hvFE models were compared with previous biomechanical tests in both stance and side-fall configurations. The influence of using the femur-specific versus a mean fabric distribution on the hvFE predictions was assessed. Femur-specific and mean fabric enhance the prediction of experimental ultimate force for the pooled, i.e. stance and side-fall, (isotropic: r^2=0.81, femur-specific fabric: r^2=0.88, mean fabric: r^2=0.86, $p < 0.001$) but not for the individual configurations. Fabric anisotropy significantly improves bone strength prediction for the pooled configurations, and mapped fabric provides a comparable prediction to true fabric. The mapping of fabric anisotropy is therefore expected to help generate more accurate QCT-based hvFE models of the proximal femur for personalised or multiple load configurations.

Keywords: anisotropy, fabric, finite element analysis, proximal femur, quantitative computed tomography, bone strength

---

Number of words: 3916

1. Introduction

Hip fractures lead to mortality, morbidity and high health care costs. The effective prevention of hip fractures requires an accurate diagnosis of osteoporosis, which is currently based on measurement of areal bone mineral density (aBMD) measured by dual energy x-ray absorptiometry (DXA). However, the majority of fractures occur in patients with aBMD above the diagnostic threshold [1, 2, 3]. This reflects the fact that aBMD alone has high specificity but low sensitivity. Alternatively, Kopperdahl et al. [4] defined femoral strength thresholds, which were based on finite element (FE) analysis, equivalent to aBMD diagnostic criterion. Based on clinical data, a combination of FE-based femoral strength and aBMD identified more individuals at high fracture risk than aBMD alone [4]. FE analysis was also shown to estimate the failure load more accurately than radiography, DXA or quantitative computed tomography (QCT) [5]. FE approaches based on computer tomography (CT) have been applied extensively throughout the past decades to simulate the mechanical behaviour of the proximal femur [6, 7, 8, 9, 10, 11, 12, 13, 14, 15, 16, 17]. With availability of quantitative CT (QCT) in hospitals, QCT-based FE analyses have been increasingly included in hip studies and clinical evaluation of drug treatments against osteoporosis [18, 19]. To evaluate the ability in predicting bone strength, QCT-based FE models of the proximal femur were validated based on mechanical tests in which proximal femora were tested in the one-legged stance [20, 21, 22, 23, 24] or unprotected side-fall configuration [25, 26, 10, 27, 14, 17]. To a lesser ex-

tent, QCT-based FE models of the proximal femur were validated in both configurations [28, 12, 29, 5].

Homogenised, voxel-based FE (hvFE) models can be generated by converting re-coarsened QCT image voxels to hexahedral cubic elements. A homogenised material property is assigned to each element that is based on a statistically representative volume element (RVE) of the material [30]. Homogenised elastic and yield properties are best predicted by bone volume fraction (BV/TV) and fabric anisotropy of trabecular bone [31, 32], but QCT images are lacking information on trabecular microstructure due to the limited resolution. Therefore, bone is usually assumed to behave isotropically in QCT-based FE models of the proximal femur [33]. Several approaches were proposed to extract fabric tensors from QCT images, but fabric anisotropy cannot be derived accurately [34, 35, 36]. On the other hand, anisotropic homogenised FE models based on high resolution peripheral QCT (HR-pQCT) improved the prediction of stiffness [11] and experimental bone strength [37, 13]. Enns-Bray et al. [14, 15] proposed a method to map femoral anisotropy from HR-pQCT into QCT-based FE models by using the direct mechanics [38] and then the mean intercept length (MIL) method [39, 40]. However, both studies involved only linear FE analyses of the proximal femur in a single load configuration. Little is known about the effect of including HR-pQCT derived fabric anisotropy into QCT-based, geometrically and materially non-linear hvFE of the human proximal femur in different loading configurations.

Alternatively, trabecular fabric anisotropy can be estimated from the HR-pQCT image of a dissected femur with multiple approaches [41, 42, 43, 44, 45]. Taghizadeh et al. [45] showed that averaged fabric anisotropy is a close approximation of patient-specific anisotropy and can be used in FE models. Chandran et al. [46] used a more systematic approach by selecting a mean femur with the closest shape and intensity to the femurs of a database (n=71). To our best knowledge, none of aforementioned approaches were tested for QCT-based hvFE models. We employed the latter single-template approach to obtain the natural fabric distribution of a mean human proximal femur and to build anisotropic hvFE models using CT scans of clinical quality. In this study, fabric anisotropy from the HR-pQCT images of the femur-specific and the mean femur were mapped to QCT-based hvFE models and non-linear FE analyses were performed to compute stiffness and strength.

The goal of this study was to assess the effect of including femur-specific or mean fabric anisotropy on the predictive ability of non-linear QCT-based hvFE models of the human proximal femur, as compared with experimentally measured stiffness and strength in two loading configurations.

2. Materials and methods

Seventy-two human proximal femora (35 males, 37 females, age 77±11 years, range 46-96 years) were obtained from body donors prepared by the Division of Anatomy of the Medical University of Vienna. Collection and preparation procedures were approved by the ethics commission of the Medi-

cal University of Vienna. Informed consent was obtained from all donors. Sample preparation, imaging and mechanical testing of femora were explained in detail by [12] and [13]. According to the calculated T-score from DXA, 29 of the femora were osteoporotic, 22 were osteopenic and 21 were normal. The procedures are explained here briefly.

2.1. Imaging and testing

QCT scanning

Each femur was scanned with a clinical QCT (Brilliance 64, Philips, Germany; intensity: 100 mA; voltage: 120 kV; voxelsize: 0.33×0.33×1.0 mm^3) with a calibration phantom (BDC phantom, QMR GmbH, Germany) for converting the Hounsfield unit (HU) scale to equivalent BMD scale in mgHA/CC. The BMD range was restricted to -100 and 1400 mgHA/cc to decrease the effect of residual air bubbles and other artefacts [12].

HR-pQCT scanning

Each femur was also scanned with an HR-pQCT (Xtreme CT, Scanco, Switzerland; intensity: 900 µA, voltage: 60 kVp, voxel size: 0.082×0.082×0.082 mm^3). The scanned images were converted from HU to BMD scale following the manufacturer's calibration procedure. Similarly to QCT, the BMD range was restricted to -100 and 1400 mgHA/cc [13].

Mechanical tests

A femur of each pair was randomly selected to be tested in a one-legged

stance and side-fall configuration. In stance configuration, the cranial portion of the femoral head was embedded in polyurethane (PU). In side-fall configuration, the medial portion of the femoral head and the lateral portion of the greater trochanter were embedded in PU. The shaft was fixed in both configurations. A custom-made bearing was used to reduce transverse forces/moments by allowing rotation and 2 translations perpendicular to the loading axis. Each femur was compressed to failure by a servo-hydraulic testing machine (Mini-Bionix, MTS system, USA) at a rate of 5 mm/min. Femoral ultimate force was defined as the maximum compressive load. The stiffness was the maximum slope of the linear part of the load-displacement curve [12].

2.2. QCT-based hvFE model generation

The QCT images of the femora were cropped proximally, upsampled along the scanning axis to isotropic voxel size of 0.33 mm, rotated to an experimental position (stance or side-fall configuration), masked and coarsened to a resolution of 3 mm. A filling out algorithm was used to find the outer contour of each image. Image processing was done with the software MED-TOOL (www.dr-pahr.at). Due to the equivalent performance of voxel and smooth mesh FE models in a recent QCT-based clinical study [47], it was decided to use the simpler voxel mesh in this study. An hvFE model of each femur was therefore generated by converting image voxels to linear hexahedron elements. Each voxel was assigned its local voxel BMD values. The

calibration relationship between BMD and BV/TV is provided in Dall'Ara et al. [12].

Image registration

Grayscale HR-pQCT images were segmented in the original coordinate system with the manufacturer's software (Scanco Medical, Switzerland). Both grayscale and segmented HR-pQCT images were pre-oriented (left/right and top/bottom) along the experimental position by using the flipping function in MIPAV software (http://mipav.cit.nih.gov). Rotated QCT images were upsampled to 82 µm isotropic voxels. In the following description of the image registration methodology, HR-pQCT and QCT images refer to pre-oriented HR-pQCT and upsampled rotated QCT images, respectively.

A mean femur closest to all the femurs of the available collection was selected. To do so, each donor femur image was registered to all the femora to quantify the distance metric based on the logarithm of the left stretch tensor of the gradient of the non-rigid transformation [46]. Based on this calculation, the femur with the minimal cumulated distance metric to all other femora was chosen to be the mean femur, which was then excluded from the analysis. Therefore, the femur dataset included the remaining 71 femora. Subsequently, image registrations were performed by using the software ELASTIX [48] to calculate two types of transformations.

1. A donor femur transformation $\boldsymbol{t}_{\mathrm{o}}$ is a rigid transformation which maps coordinates in an HR-pQCT image ($\boldsymbol{x}_{\mathrm{HRpQCT_{donor}}}$) to coordinates in the

QCT image ($\boldsymbol{x}_{\mathrm{QCT}_{\mathrm{donor}}}$) of the same donor. The expression is defined as:

$$\boldsymbol{x}_{\mathrm{QCT}_{\mathrm{donor}}} = \boldsymbol{t}_{\mathrm{o}}(\boldsymbol{x}_{\mathrm{HRpQCT}_{\mathrm{donor}}}) = \mathbf{R}_{\mathrm{o}}(\boldsymbol{x}_{\mathrm{HRpQCT}_{\mathrm{donor}}} - \boldsymbol{c}_{\mathrm{o}} - \boldsymbol{b}_{\mathrm{o}}) + \boldsymbol{c}_{\mathrm{o}} \quad (1)$$

where $\mathbf{R}_{\mathrm{o}}$, $\boldsymbol{c}_{\mathrm{o}}$, $\boldsymbol{b}_{\mathrm{o}}$ are the rotation matrix, the centre of rotation and the translation vector, respectively.

2. A mean-femur transformation $\boldsymbol{t}_{\mathrm{m}}$ combined two-step transformations from the mean-femur HR-pQCT image to a donor QCT image. First, the transformation $\boldsymbol{t}_{\mathrm{m_1}}$ is a rigid transformation which maps coordinates in the mean-femur HR-pQCT image ($\boldsymbol{x}_{\mathrm{HRpQCT}_{\mathrm{mean}}}$) to coordinates in the mean-femur QCT image ($\boldsymbol{x}_{\mathrm{QCT}_{\mathrm{mean}}}$). The expression is given by:

$$\boldsymbol{x}_{\mathrm{QCT}_{\mathrm{mean}}} = \boldsymbol{t}_{\mathrm{m_1}}(\boldsymbol{x}_{\mathrm{HRpQCT}_{\mathrm{mean}}}) = \mathbf{R}_{\mathrm{m_1}}(\boldsymbol{x}_{\mathrm{HRpQCT}_{\mathrm{mean}}} - \boldsymbol{c}_{\mathrm{m_1}} - \boldsymbol{b}_{\mathrm{m_1}}) + \boldsymbol{c}_{\mathrm{m_1}} \quad (2)$$

where $\mathbf{R}_{\mathrm{m_1}}$, $\boldsymbol{c}_{\mathrm{m_1}}$, $\boldsymbol{b}_{\mathrm{m_1}}$ were the rotation matrix, the centre of rotation and the translation vector, respectively.

Second, the transformation $\boldsymbol{t}_{\mathrm{m_2}}$ combines rigid and non-rigid (affine and b-spline) transformations from $\boldsymbol{x}_{\mathrm{QCT}_{\mathrm{mean}}}$ to $\boldsymbol{x}_{\mathrm{QCT}_{\mathrm{donor}}}$. The expression is given by:

$$\boldsymbol{x}_{\mathrm{QCT}_{\mathrm{donor}}} = \boldsymbol{t}_{\mathrm{m_2}}(\boldsymbol{x}_{\mathrm{QCT}_{\mathrm{mean}}}) = \boldsymbol{t}_{\mathrm{B}}(\boldsymbol{t}_{\mathrm{A}}(\boldsymbol{t}_{\mathrm{R}}(\boldsymbol{x}_{\mathrm{QCT}_{\mathrm{mean}}}))) \quad (3)$$

where $\boldsymbol{t}_{\mathrm{B}}$, $\boldsymbol{t}_{\mathrm{A}}$ and $\boldsymbol{t}_{\mathrm{R}}$ denote b-spline, affine, and rigid transformations,

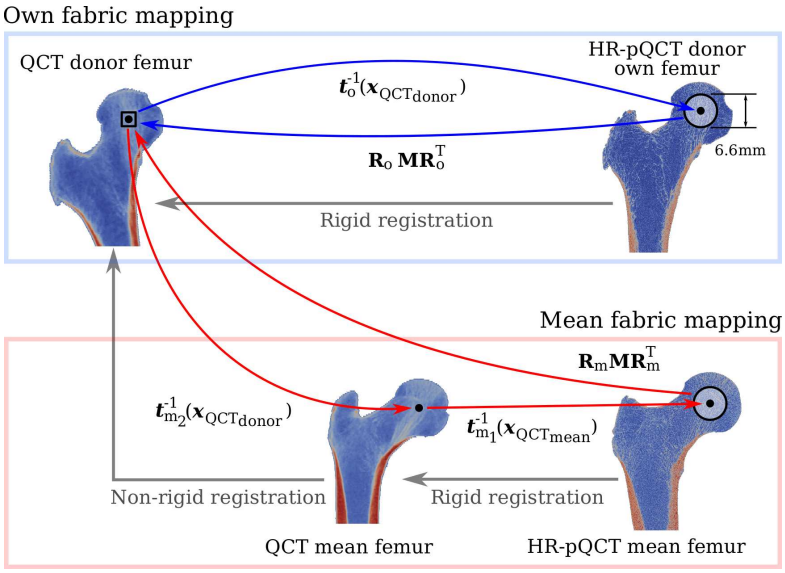

Figure 1: Fabric mapping methodology for femur-specific and mean femur HR-pQCT images. $\boldsymbol{t}_{\mathrm{o}}^{-1}$, $\boldsymbol{t}_{\mathrm{m_1}}^{-1}$ and $\boldsymbol{t}_{\mathrm{m_2}}^{-1}$ are transformations from donor QCT to donor HR-pQCT, from mean-femur QCT to mean-femur HR-pQCT and from donor QCT to mean-femur QCT image. $\mathbf{M}$ is a fabric tensor. $\mathbf{R}_{\mathrm{o}}$ and $\mathbf{R}_{\mathrm{m}}$ are rotation matrices from donor HR-pQCT to donor QCT and from mean-femur HR-pQCT to donor QCT image.

145 respectively.

Finally, the total mean-femur transformation $\boldsymbol{t}_{\mathrm{m}}$ is expressed as:

$$\boldsymbol{x}_{\mathrm{QCT_{donor}}} = \boldsymbol{t}_{\mathrm{m}}(\boldsymbol{x}_{\mathrm{HRpQCT_{mean}}}) = \boldsymbol{t}_{\mathrm{m_2}}(\boldsymbol{t}_{\mathrm{m_1}}(\boldsymbol{x}_{\mathrm{HRpQCT_{mean}}})) \tag{4}$$

Fabric mapping

Figure 1 shows the fabric mapping methodology for donor femora and mean femora. Fabric mapping was then performed for QCT images with 3 mm mesh size. For femur-specific fabric mapping, $\boldsymbol{x}_{\mathrm{QCT}_{\mathrm{donor}}}$ were mapped to $\boldsymbol{x}_{\mathrm{HRpQCT}_{\mathrm{donor}}}$ by using the transformation $\boldsymbol{t}_{\mathrm{o}}^{-1}$. For mean fabric mapping, $\boldsymbol{x}_{\mathrm{QCT}_{\mathrm{donor}}}$ were mapped to $\boldsymbol{x}_{\mathrm{QCT}_{\mathrm{mean}}}$ by using the transformation $\boldsymbol{t}_{\mathrm{m}_2}^{-1}$ and $\boldsymbol{x}_{\mathrm{QCT}_{\mathrm{mean}}}$ were mapped to $\boldsymbol{x}_{\mathrm{HRpQCT}_{\mathrm{mean}}}$ by using the transformation $\boldsymbol{t}_{\mathrm{m}_1}^{-1}$. In the HR-pQCT image, a fabric tensor was calculated over a spherical RVE by using the MIL method. The spherical RVE had a diameter of 6.6 mm which had the same volume as a cube with 5.3 mm edge length used in trabecular bone homogenisation [49, 50, 51]. Then, the fabric tensor was rotated back to the coordinate system of the donor QCT image by using $\mathbf{R}_{\mathrm{o}}$ for the femur-specific fabric mapping and $\mathbf{R}_{\mathrm{m}}$ for the mean fabric mapping, where $\mathbf{R}_{\mathrm{m}} = \mathbf{R}_{\mathrm{m}_2}\mathbf{R}_{\mathrm{m}_1}$ and $\mathbf{R}_{\mathrm{m}_2}$ was the rotation matrix derived from the polar decomposition $\mathbf{RU}$ of the gradient of the transformation $\boldsymbol{t}_{\mathrm{m}_2}$ [52].

Embedding and FE model generation

A PU and a steel layer of cylindrical shape were modelled as in the experimental setup shown in Fig. 2. hvFE models of the proximal femur were generated by converting image down-sampled voxels (3 mm^3) to hexahedral cubic elements.

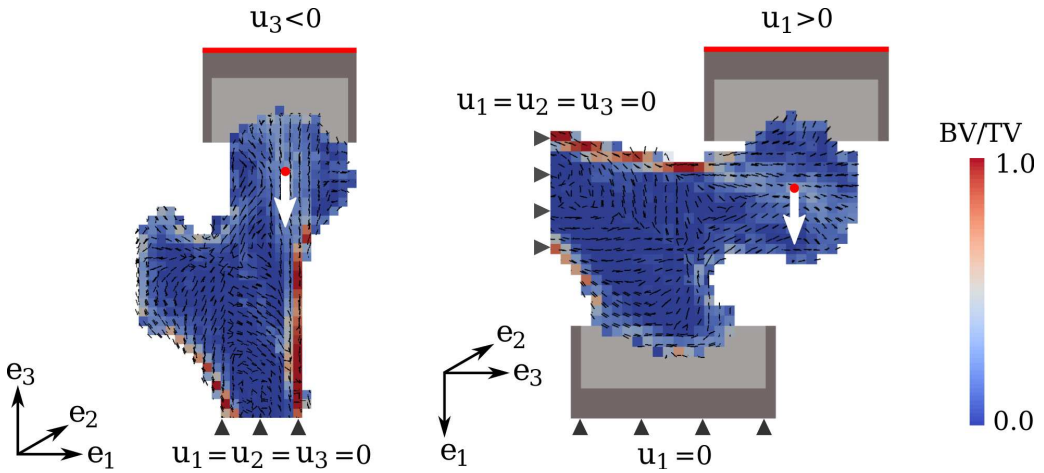

Figure 2: Homogenised voxel FE models in stance and side-fall configurations. The principle direction of mean fabric tensors is illustrated by small black lines. u_i and e_i are displacements and unit directions. The displacement was applied on the reference node at the centre of the femoral head (red dot) which was coupled with the embedding boundary (red line).

Boundary conditions

The boundary conditions were improved with respect to the original FE analyses of Dall'Ara et al. [12]. The lever arm of the applied force was maintained in the centre of the femoral head to account for the motion between the loading cup and the articular cartilage. The radius of each femoral head was computed by fitting a sphere to the femoral head using BoneJ, a plugin in ImageJ [53, 54]. A reference node at the center of the femoral head was kinematically coupled with the top surface of the loading cups and constrained with a displacement in the loading direction only. In-plane translations and rotations were left free to simulate the experimental setup. In side-fall configuration, the most lateral surface of the steel embedding below the greater trochanter was fixed only in the loading direction. In both configurations,

Table 1: Elasticity and strength model parameters

	Elasticity					Strength		
Variable	ε_0	ν_0	μ_0	k	l	σ_0	χ_0	τ_0
Unit	[MPa]	[-]	[MPa]	[-]	[-]	[MPa]	[-]	[MPa]
Tension (+)	6614	0.246	2654	1.33	1.0	54.8	-0.246	44.6
Compression (-)						72.9	0.333	

the distal surface of the shaft was fixed in all directions.

Material properties

The material properties of the embedding were assumed isotropic with Poisson ratio 0.3. PU elements were assigned Young's modulus 1.36 GPa and steel elements 210 GPa. The elastic-damage constitutive law was adapted from [55] which includes volume fraction and fabric-based elasticity [56] and a piecewise Hill yield criterion [57]. Table 1 shows the anisotropic material constants taken from [58] and applied to the axial compression of vertebral body sections in [59]. The material properties of cortical bone were extrapolated from those of trabecular bone by using a nonlinear but smooth tissue function [12]. At BV/TV = 1, the elastic modulus equals 24 GPa, the compressive strength 266 MPa and the tensile strength equals 200 MPa. An exponential hardening law was applied. The damage variable is an exponential function of the cumulated plastic strain and represents the progressive failure of the bone element and ranges from 0 (intact) to 1 (failed) [55].

FE analyses

Nonlinear FE analyses were performed by using Abaqus (Abaqus 2016, Simulia, Dassault Systemes, Velizy-Villacoublay, France) until the maximum displacement was reached. FE stiffness was defined as the slope in the first steps and ultimate load as the maximum force in the force-displacement curve. The damage variable was computed in each element at every step.

Linear regressions of the relationship between computed and experimental results (i.e. ultimate force and stiffness) of pooled (combined stance and side-fall) configurations and the two individual load configurations were calculated for comparison. The significance level was set to $p < 0.05$ and the correlation coefficients r^2 were compared by using William's formula [60].

3. Results

Fabric anisotropy significantly improved the prediction of experimental ultimate force in pooled configurations. Correlation r^2 between hvFE and experimental ultimate force increased from 0.81 to 0.88 ($p < 0.001$) for femur-specific fabric and to 0.86 ($p < 0.001$) for mean fabric (Table 2). Prediction of isotropic hvFE models were equivalent to hvFE models from Dall'Ara et al. [12]. In single load configurations, anisotropy did not improve the predictions (stance: r^2 from 0.82 to 0.84 with $p = 0.1$). Regression lines of anisotropic models were closer to the 1:1 line compared to isotropic models (isotropic: $y = 1.6x - 0.369$, femur-specific fabric: $y = 1.1x + 0.134$, mean fabric: $y = 1.2x + 0.388$). Table 3 shows the correlation coefficients r^2

Table 2: Prediction of ultimate force. Coefficients of determination r^2 and standard errors of the estimate (SEE) of the linear regressions of the relationships between hvFE and experimental ultimate force in pooled stance and side-fall configurations, stance configuration and side-fall configuration. Comparison was made with previous studies on the same collection of femora.

	r^2			SEE [kN]		
	pooled	stance	fall	pooled	stance	fall
QCT [12]						
Isotropic	0.80	0.80	0.85	1.58	1.28	0.44
QCT Present study						
Isotropic	0.81	0.82	0.87	1.58	1.32	0.41
Anisotropic: mean fabric	0.86	0.80	0.85	1.33	1.31	0.44
Anisotropic: femur-specific fabric	0.88	0.84	0.86	1.22	1.15	0.42
HR-pQCT [13]						
Anisotropic: femur-specific fabric	0.88	0.87	0.86	1.17	1.19	0.64

and the standard errors of the estimate (SEE) of linear regressions between hvFE and experimental stiffness for pooled and single configurations. Femur-specific fabric improved the correlations in pooled ($p < 0.001$) and stance configurations. The regression equations of the isotropic models, anisotropic models with femur-specific fabric and anisotropic models with mean fabric were $y = 0.76x + 0.329$, $y = 0.61x + 0.365$ and $y = 0.62x + 0.547$, respectively. Examples of damage distribution at ultimate force in both stance and side-fall configurations are shown in Fig. 3.

4. Discussion

This study evaluates non-linear anisotropic QCT-based hvFE models of the human proximal femur for the first time. The computed FE ultimate force and stiffness of 71 femora in both stance and side-fall configurations

Table 3: Prediction of stiffness. Coefficients of determination r^2 and standard errors of the estimate (SEE) of the linear regressions of the relationships between hvFE and experimental stiffness in pooled stance and side-fall configurations, stance configuration and side-fall configuration. Comparison was made with previous studies on the same collection of femora.

	r^2			SEE [kN]		
	pooled	stance	fall	pooled	stance	fall
QCT [12]						
Isotropic	0.90	0.82	0.74	0.88	0.91	0.23
QCT Present study						
Isotropic	0.90	0.82	0.79	0.89	1.35	0.21
Anisotropic: mean fabric	0.91	0.81	0.76	0.84	4.77	0.23
Anisotropic: femur-specific fabric	0.93	0.84	0.78	0.76	1.51	0.22
HR-pQCT [13]						
Anisotropic: femur-specific fabric	0.92	0.86	0.80	0.78	0.73	0.21

were compared with experimental results from Dall'Ara et al. [12]. The set of femora has a broad spectrum of age and T-score, which supports the generality of the findings. As expected, isotropic models of the current study and those of Dall'Ara et al. [12] predict experimental ultimate forces similarly (Table 2). The minor improvements of the correlation coefficients obtained in the present study are most probably due to the more realistic reproduction of the experimental boundary conditions.

Anisotropy significantly improves prediction (r^2) of experimental ultimate force in pooled configurations by 7 % for femur-specific fabric and 5 % for mean fabric compared to isotropic models ($r^2 = 0.81$). The small difference between femur-specific and mean fabric confirms the ability of the mapping algorithm to produce an approximate but realistic trabecular orientation in the QCT-based FE models [46].

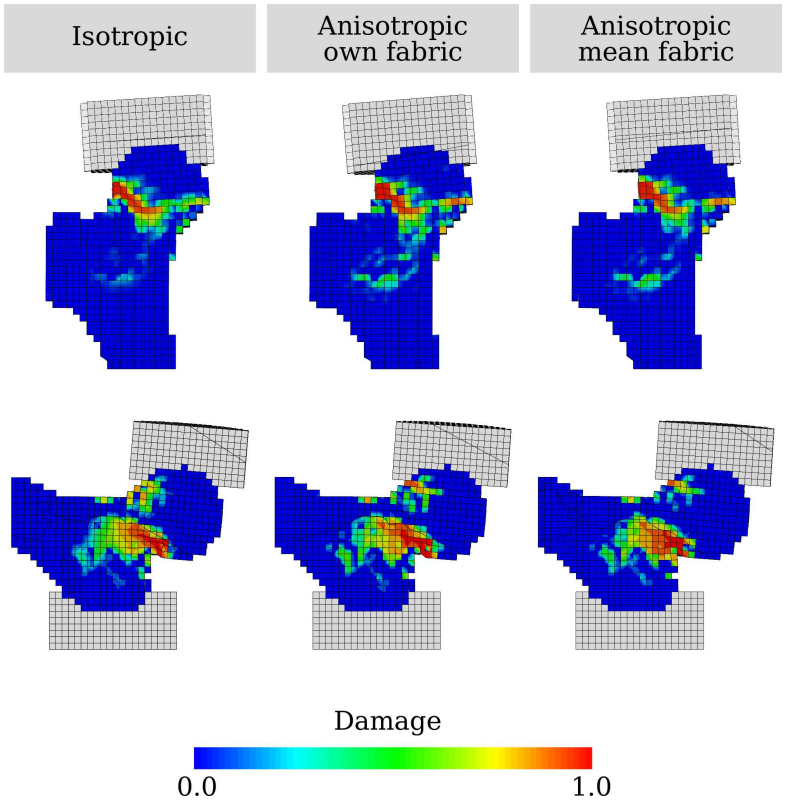

Figure 3: Damage at ultimate force obtained with the isotropic and anisotropic with femur-specific or mean fabric hvFE models.

Nevertheless, mean fabric enhances prediction of bone strength in pooled configurations. This shows that HR-pQCT mean-fabric template could benefit the hvFE analysis of the proximal femur in clinical CT images, where the femur-specific fabric is not available. In the side-fall configuration, the effect of anisotropy is negligible. This agrees well with the finding of [13] and [14]. In fact, the stress distribution of the side-fall load configuration does not align with the main compressive trabecular bundle of the proximal femur and is therefore less sensitive to fabric. In addition, QCT-based hvFE

may simply not properly capture the architecture of the later cortex failing in compression in the fall configuration.

However, patients fall in various configurations. The validation for pooled configurations prevents over-fitting the FE models to a specific load configuration. As anisotropy helps align the regression lines of the two load configurations, it suggests that the methodology to generate anisotropic QCT-based FE models of the proximal femur is more general and could be valid for other clinically relevant load configurations.

Compared to published FE analyses of the proximal femur, the strength prediction ability of anisotropic hvFE models using femur-specific fabric is in the mid-range for pooled cases (r^2=0.80-0.94) [28, 12, 13, 29, 5] and for stance cases (r^2=0.75-0.96), and is in the upper range for side-fall cases (r^2=0.73-0.90) [61, 19, 33]. In particular, these predictions are comparable to HR-pQCT-based homogenised smooth FE (hsFE) models of [13] which are slightly better in stance configuration (hvFE: r^2=0.84, hsFE: r^2=0.87) but equivalent in pooled and side-fall (r^2=0.86) configurations.

The hvFE models of the current study explain more than 90 % of experimental bone stiffness for the pooled loading cases. In stance case, anisotropic models predict stiffness better than published FE models (r^2=0.62-0.82) [23, 12] and are in the mid-range for side-fall cases (r^2=0.72-0.87) [14, 15, 33, 17]. The results show that hvFE models overestimate experimental stiffness. However, the measured stiffness in biomechanical tests could be lower than the actual stiffness due to the presence of a compliant cartilage layer around

the femoral head in the experiments [12].

The results suggest also that hvFE models underestimate ultimate load. The anisotropic material constants of ultimate strength are taken from [62] and may indeed require a correction for the different *in situ* boundary conditions [63] associated with the loading of the whole proximal femur. The mesh size of 3 mm was shown to be a good compromise for hvFE models. On the one hand, this element size is larger than cortical thickness and smaller than the trabecular biopsies side-length of 5.3 mm used for homogenisation of elastic and yield properties by [49, 51]. Nevertheless, it provides a comparable prediction to HR-pQCT-based homogenised, smooth finite element (hsFE) models.

We investigated the mesh convergence behaviour for stiffness by refining the isotropic hvFE models from 3 mm to 1.5 mm and 1 mm. The reference images for the assignment of material properties remained identical to exclude the influence of material property mapping in the convergence analysis. The stiffness difference between 3 mm and 1.5 mm meshes were 6.4 %, and between 1.5 mm and 1 mm meshes 1.6 %. This indicates that stiffness computed with 3 mm voxels remained within approximately 10% of the one calculated with a converged voxel mesh. Given the usual close relationship between FE stiffness and ultimate load, we expect this convergence behaviour for stiffness to remain in the same order of magnitude for ultimate load. Nevertheless, when considering anisotropic hvFE models with 1.5 mm mesh size, the regression curve between experimental and hvFE ultimate forces did not

match the 1:1 relationship. This may be due to other factors such as the distinct representative volume element size in cortical and trabecular regions. In addition, mesh refinement (from 3 mm to 1.5 mm) did not improve prediction of anisotropic models in pooled configurations. This indicates that anisotropy dominates the reconciliation of the strength prediction between the stance and side-fall load cases.

In addition, the 3 mm models were cost-effective. They took only 7 GB memory and 20 minutes CPU time for a non-linear analysis which could be performed on a normal desktop PC. Finer meshes required a more powerful computing machine. The 1.5 mm mesh required 12 GB memory and 4 hours CPU time for a non-linear analysis. The 1 mm mesh took up to 50 GB memory and 5 hours for a single-step linear FE analysis.

There are some limitations in this study. First, the hvFE models generated in this study are specific for the *in vitro* mechanical testing from Dall'Ara et al. [12]. QCT images of isolated proximal femora are not rigorously equivalent to QCT images of the same skeletal element *in vivo*. Second, due to the presence of the cartilage interface, the experimental setup led to lower measured stiffness compared to the simulated bone stiffness. Consequently, elastic properties of hvFE models cannot be validated properly. Third, the cortex surrounding the proximal femur cannot be properly represented by 3 mm voxels. This limitation could be circumvented by using methods that were proposed to extract cortical thickness from QCT images [64, 65]. For accurate modelling of the cortical shell, smooth wedge elements

may be used [13]. Fourth, the RVE size for trabecular bone and cortical bone were identical. When trabecular and cortical layers could be modelled separately, different RVE size for each layer could be adjusted to achieve better predictions. Fifth, the mean femur template used to map anisotropy in this study is specific to the available collection of 71 femora and may need to be generalised to larger collections of femora in future clinical applications. Lastly, material properties were not fine-tuned but directly taken from [62]. This was not the focus of this study but a proper tuning could obviously align prediction curve with the 1:1 relationship.

In this study, non-linear anisotropic QCT-based hvFE models of the proximal femur in pooled stance and side-fall configurations were validated for the first time. Anisotropy improves significantly bone strength and stiffness prediction in pooled configurations, and the prediction of mean-fabric template is comparable to femur-specific fabric. This suggests that mapping mean fabric-anisotropy could help generate QCT-based hvFE models of the proximal femur for clinical application. In future studies, the influence of the cortical layer in QCT-based hvFE needs to be investigated by modelling cortical and trabecular regions separately. This could be achieved by using smooth wedge or shell elements of variable thickness. Additionally, a proper RVE size and material constants need to be defined for each compartment. More accurate FE models are expected to enhance accuracy of femoral strength prediction and the associated fracture risk assessment.

Acknowledgements The authors would like to thank Dr. Vimal Chandran for providing the image registration methodology and Dr. Elham Taghizadeh for insightful discussion in fabric mapping. The simulations were performed on the Ubelix cluster of the University of Bern. This research was supported by grant no 143769 of the Swiss National Science Foundation.

Declarations The authors have no conflicts of interests.

References

[1] J. A. Kanis, O. Johnell, A. Oden, C. De Laet, B. Jonsson, A. Dawson, Ten-year risk of osteoporotic fracture and the effect of risk factors on screening strategies, Bone 30 (1) (2002) 251–258. doi:10.1016/S8756-3282(01)00653-6.

[2] S. C. E. Schuit, M. van der Klift, A. E. A. M. Weel, C. E. D. H. de Laet, H. Burger, E. Seeman, A. Hofman, A. G. Uitterlinden, J. P. T. M. van Leeuwen, H. A. P. Pols, Fracture incidence and association with bone mineral density in elderly men and women: the Rotterdam Study, Bone 34 (1) (2004) 195–202. doi:10.1016/j.bone.2003.10.001.

[3] L. Langsetmo, D. Goltzman, C. S. Kovacs, J. D. Adachi, D. A. Hanley, N. Kreiger, R. Josse, A. Papaioannou, W. P. Olszynski, S. A. Jamal, Repeat Low-Trauma Fractures Occur Frequently Among Men and Women Who Have Osteopenic BMD, Journal of Bone and Mineral Research 24 (9) (2009) 1515–1522. doi:10.1359/jbmr.090319.

[4] D. L. Kopperdahl, T. Aspelund, P. F. Hoffmann, S. Sigurdsson, K. Siggeirsdottir, T. B. Harris, V. Gudnason, T. M. Keaveny, Assessment of Incident Spine and Hip Fractures in Women and Men using Finite Element Analysis of CT Scans, Journal of bone and mineral research : the official journal of the American Society for Bone and Mineral Research 29 (3) (2014) 570–580. doi:10.1002/jbmr.2069.

[5] P. Pottecher, K. Engelke, L. Duchemin, O. Museyko, T. Moser, D. Mitton, E. Vicaut, J. Adams, W. Skalli, J. D. Laredo, V. Bousson, Prediction of Hip Failure Load: In Vitro Study of 80 Femurs Using Three Imaging Methods and Finite Element ModelsThe European Fracture Study (EFFECT), Radiology (2016) 142796doi:10.1148/radiol.2016142796.

[6] J. Keyak, M. Fourkas, J. Meagher, H. Skinner, Validation of an automated method of three-dimensional finite element modelling of bone., Journal of Biomedical Engineering 15 (6) (1993) 505–9.

[7] B. Merz, P. Niederer, R. Muller, P. Ruegsegger, Automated finite element analysis of excised human femora based on precision -QCT., Journal of Biomechanical Engineering 118 (3) (1996) 387–90.

[8] D. Cody, F. Hou, G. Divine, D. Fyhrie, Short term in vivo precision of proximal femoral finite element modeling.[Erratum appears in Ann Biomed Eng 2000 Nov-Dec;28(11):1397], Annals of Biomedical Engineering 28 (4) (2000) 408–14.

[9] T. M. Keaveny, P. F. Hoffmann, M. Singh, L. Palermo, J. P. Bilezikian, S. L. Greenspan, D. M. Black, Femoral Bone Strength and Its Relation to Cortical and Trabecular Changes After Treatment With PTH, Alendronate, and Their Combination as Assessed by Finite Element Analysis of Quantitative CT Scans, Journal of Bone and Mineral Research 23 (12) (2008) 1974–1982. doi:10.1359/jbmr.080805.

[10] L. Grassi, E. Schileo, F. Taddei, L. Zani, M. Juszczyk, L. Cristofolini, M. Viceconti, Accuracy of finite element predictions in sideways load configurations for the proximal human femur, Journal of Biomechanics 45 (2) (2012) 394–399. doi:10.1016/j.jbiomech.2011.10.019.

[11] J. Hazrati Marangalou, K. Ito, B. van Rietbergen, A new approach to determine the accuracy of morphologyelasticity relationships in continuum FE analyses of human proximal femur, Journal of Biomechanics 45 (16) (2012) 2884–2892. doi:10.1016/j.jbiomech.2012.08.022.

[12] E. Dall'Ara, B. Luisier, R. Schmidt, F. Kainberger, P. Zysset, D. Pahr, A nonlinear QCT-based finite element model validation study for the human femur tested in two configurations in vitro, Bone 52 (1) (2013) 27–38. doi:10.1016/j.bone.2012.09.006.

[13] B. Luisier, E. DallAra, D. H. Pahr, Orthotropic HR-pQCT-based FE models improve strength predictions for stance but not for side-way fall loading compared to isotropic QCT-based FE models of human femurs, Journal of the Mechanical Behavior of Biomedical Materials 32 (2014) 287–299. doi:10.1016/j.jmbbm.2014.01.006.

[14] W. S. Enns-Bray, J. S. Owoc, K. K. Nishiyama, S. K. Boyd, Mapping anisotropy of the proximal femur for enhanced image based finite element analysis, Journal of Biomechanics 47 (13) (2014) 3272–3278. doi:10.1016/j.jbiomech.2014.08.020.

[15] W. S. Enns-Bray, O. Ariza, S. Gilchrist, R. P. Widmer Soyka, P. J. Vogt, H. Palsson, S. K. Boyd, P. Guy, P. A. Cripton, S. J. Ferguson, B. Helgason, Morphology based anisotropic finite element models of the proximal femur validated with experimental data, Medical Engineering & Physics 38 (11) (2016) 1339–1347. doi:10.1016/j.medengphy.2016.08.010.

[16] M. Qasim, G. Farinella, J. Zhang, X. Li, L. Yang, R. Eastell, M. Viceconti, Patient-specific finite element estimated femur strength as a predictor of the risk of hip fracture: the effect of methodological determinants, Osteoporosis International (2016) 1–8doi:10.1007/s00198-016-3597-4.

[17] F. Johannesdottir, E. Thrall, J. Muller, T. M. Keaveny, D. L. Kopperdahl, M. L. Bouxsein, Comparison of non-invasive assessments of strength of the proximal femur, Bonedoi:10.1016/j.bone.2017.07.023.

[18] K. Engelke, T. Lang, S. Khosla, L. Qin, P. Zysset, W. D. Leslie, J. A. Shepherd, J. T. Schousboe, Clinical Use of Quantitative Computed Tomography (QCT) of the Hip in the Management of Osteoporosis in Adults: the 2015 ISCD Official PositionsPart I, Journal of Clinical Densitometry 18 (3) (2015) 338–358. doi:10.1016/j.jocd.2015.06.012.

[19] P. Zysset, L. Qin, T. Lang, S. Khosla, W. D. Leslie, J. A. Shepherd, J. T. Schousboe, K. Engelke, Clinical Use of Quantitative Computed TomographyBased Finite Element Analysis of the Hip and Spine in the

Management of Osteoporosis in Adults: the 2015 ISCD Official PositionsPart II, Journal of Clinical Densitometry 18 (3) (2015) 359–392. doi:10.1016/j.jocd.2015.06.011.

[20] D. D. Cody, G. J. Gross, F. J. Hou, H. J. Spencer, S. A. Goldstein, D. P. Fyhrie, Femoral strength is better predicted by finite element models than QCT and DXA, Journal of Biomechanics 32 (10) (1999) 1013–1020. doi:10.1016/S0021-9290(99)00099-8.

[21] J. Keyak, Improved prediction of proximal femoral fracture load using nonlinear finite element models, Medical Engineering & Physics 23 (3) (2001) 165–173. doi:10.1016/S1350-4533(01)00045-5.

[22] M. Bessho, I. Ohnishi, J. Matsuyama, T. Matsumoto, K. Imai, K. Nakamura, Prediction of strength and strain of the proximal femur by a CT-based finite element method, Journal of Biomechanics 40 (8) (2007) 1745–1753. doi:10.1016/j.jbiomech.2006.08.003.

[23] L. Duchemin, D. Mitton, E. Jolivet, V. Bousson, J. Laredo, W. Skalli, An anatomical subject-specific FE-model for hip fracture load prediction., Computer Methods in Biomechanics & Biomedical Engineering 11 (2) (2008) 105–11.

[24] R. Hambli, E. Lespessailles, C.-L. Benhamou, Integrated remodeling-to-fracture finite element model of human proximal femur behavior, Journal

of the Mechanical Behavior of Biomedical Materials 17 (2013) 89–106. doi:10.1016/j.jmbbm.2012.08.011.

[25] D. Dragomir-Daescu, J. O. D. Buijs, S. McEligot, Y. Dai, R. C. Entwistle, C. Salas, L. J. M. Iii, K. E. Bennet, S. Khosla, S. Amin, Robust QCT/FEA Models of Proximal Femur Stiffness and Fracture Load During a Sideways Fall on the Hip, Annals of Biomedical Engineering 39 (2) (2011) 742–755. doi:10.1007/s10439-010-0196-y.

[26] J. E. Koivumäki, J. Thevenot, P. Pulkkinen, V. Kuhn, T. M. Link, F. Eckstein, T. Jämsä, Ct-based finite element models can be used to estimate experimentally measured failure loads in the proximal femur, Bone 50 (4) (2012) 824–829. doi:10.1016/j.bone.2012.01.012.

[27] K. K. Nishiyama, S. Gilchrist, P. Guy, P. Cripton, S. K. Boyd, Proximal femur bone strength estimated by a computationally fast finite element analysis in a sideways fall configuration, Journal of Biomechanics 46 (7) (2013) 1231–1236. doi:10.1016/j.jbiomech.2013.02.025.

[28] J. H. Keyak, S. A. Rossi, K. A. Jones, H. B. Skinner, Prediction of femoral fracture load using automated finite element modeling, Journal of Biomechanics 31 (2) (1998) 125–133. doi:10.1016/S0021-9290(97)00123-1.

[29] E. Schileo, L. Balistreri, L. Grassi, L. Cristofolini, F. Taddei, To what extent can linear finite element models of human femora predict failure

under stance and fall loading configurations?, Journal of Biomechanics 47 (14) (2014) 3531–3538. doi:10.1016/j.jbiomech.2014.08.024.

[30] T. Harrigan, M. Jasty, R. Mann, W. Harris, Limitations of the continuum assumption in cancellous bone, Journal of Biomechanics 21 (4) (1988) 269–275.

[31] G. Maquer, S. N. Musy, J. Wandel, T. Gross, P. K. Zysset, Bone Volume Fraction and Fabric Anisotropy Are Better Determinants of Trabecular Bone Stiffness than Other Morphological Variables, Journal of Bone and Mineral Research (2015) n/a–n/adoi:10.1002/jbmr.2437.

[32] S. N. Musy, G. Maquer, J. Panyasantisuk, J. Wandel, P. K. Zysset, Not only stiffness, but also yield strength of the trabecular structure determined by non-linear FE is best predicted by bone volume fraction and fabric tensor, Journal of the Mechanical Behavior of Biomedical Materials 65 (2017) 808–813. doi:10.1016/j.jmbbm.2016.10.004.

[33] B. Helgason, S. Gilchrist, O. Ariza, P. Vogt, W. Enns-Bray, R. P. Widmer, T. Fitze, H. Plsson, Y. Pauchard, P. Guy, S. J. Ferguson, P. A. Cripton, The influence of the modulusdensity relationship and the material mapping method on the simulated mechanical response of the proximal femur in side-ways fall loading configuration, Medical Engineering & Physics 38 (7) (2016) 679–689. doi:10.1016/j.medengphy.2016.03.006.

[34] Z. Tabor, R. Petryniak, Z. Lataa, T. Konopka, The potential of

multi-slice computed tomography based quantification of the structural anisotropy of vertebral trabecular bone, Medical Engineering & Physics 35 (1) (2013) 7–15. doi:10.1016/j.medengphy.2012.03.003.

[35] M. E. Kersh, P. K. Zysset, D. H. Pahr, U. Wolfram, D. Larsson, M. G. Pandy, Measurement of structural anisotropy in femoral trabecular bone using clinical-resolution CT images, Journal of Biomechanics 46 (15) (2013) 2659–2666. doi:10.1016/j.jbiomech.2013.07.047.

[36] D. Larsson, B. Luisier, M. E. Kersh, E. Dall'ara, P. K. Zysset, M. G. Pandy, D. H. Pahr, Assessment of transverse isotropy in clinical-level ct images of trabecular bone using the gradient structure tensor, Ann Biomed Eng 42 (5) (2014) 950–9.

[37] D. H. Pahr, E. Dall'Ara, P. Varga, P. K. Zysset, HR-pQCT-based homogenised finite element models provide quantitative predictions of experimental vertebral body stiffness and strength with the same accuracy as FE models, Computer Methods in Biomechanics and Biomedical Engineering 15 (7) (2012) 711–720. doi:10.1080/10255842.2011.556627.

[38] B. Van Rietbergen, A. Odgaard, J. Kabel, R. Huiskes, Direct mechanics assessment of elastic symmetries and properties of trabecular bone architecture, Journal of Biomechanics 29 (12) (1996) 1653–1657. doi:10.1016/S0021-9290(96)80021-2.

[39] W. J. Whitehouse, The quantitative morphology of anisotropic

trabecular bone, Journal of Microscopy 101 (2) (1974) 153–168. doi:10.1111/j.1365-2818.1974.tb03878.x.

[40] T. P. Harrigan, R. W. Mann, Characterization of microstructural anisotropy in orthotropic materials using a second rank tensor, Journal of Materials Science 19 (3) (1984) 761–767. doi:10.1007/BF00540446.

[41] J. H. Marangalou, K. Ito, M. Cataldi, F. Taddei, B. v. Rietbergen, A novel approach to estimate trabecular bone anisotropy using a database approach, Journal of Biomechanics 46 (14) (2013) 2356–2362. doi:10.1016/j.jbiomech.2013.07.042.

[42] K. Lekadir, C. Noble, J. Hazrati-Marangalou, C. Hoogendoorn, B. v. Rietbergen, Z. A. Taylor, A. F. Frangi, Patient-Specific Biomechanical Modeling of Bone Strength Using Statistically-Derived Fabric Tensors, Annals of Biomedical Engineering 44 (1) (2015) 234–246. doi:10.1007/s10439-015-1432-2.

[43] V. Chandran, P. K. Zysset, M. Reyes, Prediction of Trabecular Bone Anisotropy from Quantitative Computed Tomography Using Supervised Learning and a Novel Morphometric Feature Descriptor, in: N. Navab, J. Hornegger, W. M. Wells, A. F. Frangi (Eds.), Medical Image Computing and Computer-Assisted Intervention – MICCAI 2015, no. 9349 in Lecture Notes in Computer Science, Springer International Publishing, 2015, pp. 621–628, dOI: 10.1007/978-3-319-24553-9_76.

[44] E. Taghizadeh, M. Reyes, P. Zysset, A. Latypova, A. Terrier, P. Büchler, Biomechanical Role of Bone Anisotropy Estimated on Clinical CT Scans by Image Registration, Annals of Biomedical Engineering (2016) 1–13doi:10.1007/s10439-016-1551-4.

[45] E. Taghizadeh, V. Chandran, M. Reyes, P. Zysset, P. Büchler, Statistical analysis of the inter-individual variations of the bone shape, volume fraction and fabric and their correlations in the proximal femur, Bonedoi:10.1016/j.bone.2017.07.012.

[46] V. Chandran, M. Reyes, P. Zysset, A novel registration-based methodology for prediction of trabecular bone fabric from clinical qct: A comprehensive analysis, PLoS One 12 (11).

[47] P. Zysset, D. Pahr, K. Engelke, H. K. Genant, M. R. McClung, D. L. Kendler, C. Recknor, M. Kinzl, J. Schwiedrzik, O. Museyko, A. Wang, C. Libanati, Comparison of proximal femur and vertebral body strength improvements in the freedom trial using an alternative finite element methodology, Bone 81 (2015) 122–130.

[48] S. Klein, M. Staring, K. Murphy, M. A. Viergever, J. P. W. Pluim, elastix: A Toolbox for Intensity-Based Medical Image Registration, IEEE Transactions on Medical Imaging 29 (1) (2010) 196–205. doi:10.1109/TMI.2009.2035616.

[49] D. Pahr, P. Zysset, Influence of boundary conditions on computed ap-

parent elastic properties of cancellous bone., Biomechanics & Modeling in Mechanobiology 7 (6) (2008) 463–76.

[50] T. Gross, D. H. Pahr, P. K. Zysset, Morphology-elasticity relationships using decreasing fabric information of human trabecular bone from three major anatomical locations, Biomechanics and modeling in mechanobiology 12 (4) (2013) 793–800. doi:10.1007/s10237-012-0443-2.

[51] J. Panyasantisuk, D. H. Pahr, P. K. Zysset, Effect of boundary conditions on yield properties of human femoral trabecular bone, Biomechanics and Modeling in Mechanobiology (2015) 1–11doi:10.1007/s10237-015-0741-6.

[52] V. Chandran, P. Zysset, M. Reyes, Prediction of trabecular bone anisotropy from quantitative computed tomography using supervised learning and a novel morphometric feature descriptor, in: Medical Image Computing and Computer-Assisted Intervention - Miccai 2015, Pt I, Vol. 9349, 2015, pp. 621–628.

[53] M. Doube, M. M. Kosowski, I. Arganda-Carreras, F. P. Cordelires, R. P. Dougherty, J. S. Jackson, B. Schmid, J. R. Hutchinson, S. J. Shefelbine, BoneJ: Free and extensible bone image analysis in ImageJ, Bone 47 (6) (2010) 1076–1079. doi:10.1016/j.bone.2010.08.023.

[54] C. A. Schneider, W. S. Rasband, K. W. Eliceiri, NIH Image to Im-

ageJ: 25 years of image analysis, Nature Methods 9 (7) (2012) 671–675. doi:10.1038/nmeth.2089.

[55] D. Garcia, P. K. Zysset, M. Charlebois, A. Curnier, A three-dimensional elastic plastic damage constitutive law for bone tissue, Biomechanics and Modeling in Mechanobiology 8 (2) (2008) 149–165. doi:10.1007/s10237-008-0125-2.

[56] P. K. Zysset, A review of morphologyelasticity relationships in human trabecular bone: theories and experiments, Journal of Biomechanics 36 (10) (2003) 1469–1485. doi:10.1016/S0021-9290(03)00128-3.

[57] P. Zysset, L. Rincón, An Alternative Fabric-based Yield and Failure Criterion for Trabecular Bone, in: P. G. A. Holzapfel, P. R. W. Ogden (Eds.), Mechanics of Biological Tissue, Springer Berlin Heidelberg, 2006, pp. 457–470.

[58] L. Rincón-Kohli, P. K. Zysset, Multi-axial mechanical properties of human trabecular bone, Biomechanics and Modeling in Mechanobiology 8 (3) (2008) 195–208. doi:10.1007/s10237-008-0128-z.

[59] D. H. Pahr, J. Schwiedrzik, E. Dall'Ara, P. K. Zysset, Clinical versus pre-clinical FE models for vertebral body strength predictions, Journal of the Mechanical Behavior of Biomedical Materials 33 (2014) 76–83. doi:10.1016/j.jmbbm.2012.11.018.

[60] J. H. Steiger, Tests for comparing elements of a correlation matrix., Psychological bulletin 87 (2) (1980) 245.

[61] S. van den Munckhof, A. A. Zadpoor, How accurately can we predict the fracture load of the proximal femur using finite element models?, Clinical Biomechanics 29 (4) (2014) 373–380. doi:10.1016/j.clinbiomech.2013.12.018.

[62] L. Rincon-Kohli, P. K. Zysset, Multi-axial mechanical properties of human trabecular bone, Biomechanics and Modeling in Mechanobiology 8 (3) (2009) 195–208.

[63] P. Wili, G. Maquer, J. Panyasantisuk, P. K. Zysset, Estimation of the effective yield properties of human trabecular bone using nonlinear micro-finite element analyses, Biomech Model Mechanobiol 16 (6) (2017) 1925–1936.

[64] G. M. Treece, A. H. Gee, Independent measurement of femoral cortical thickness and cortical bone density using clinical CT, Medical Image Analysis 20 (1) (2015) 249–264. doi:10.1016/j.media.2014.11.012.

[65] O. Museyko, B. Gerner, K. Engelke, Cortical Bone Thickness Estimation in CT Images: A Model-Based Approach Without Profile Fitting, in: Computational Methods and Clinical Applications for Spine Imaging, Springer International Publishing, 2016.